Journal of Power Sources 196 (2011) 449–457

Contents lists available at ScienceDirect

Journal of Power Sources

journal homepage: www.elsevier.com/locate/jpowsour

# Electro-thermal battery model identification for automotive applications

Y. Hu, S. Yurkovich*, Y. Guezennec, B.J. Yurkovich

*Center for Automotive Research, The Ohio State University, 930 Kineear Rd, Columbus, OH 43212, United States*

ARTICLE INFO

*Article history:*
Received 26 April 2010
Accepted 14 June 2010
Available online 22 June 2010

*Keywords:*
Hybrid vehicles
Battery
Lithium ion
Modeling
System identification
Automotive

ABSTRACT

This paper describes a model identification procedure for identifying an electro-thermal model of lithium ion batteries used in automotive applications. The dynamic model structure adopted is based on an equivalent circuit model whose parameters are scheduled on the state-of-charge, temperature, and current direction. Linear spline functions are used as the functional form for the parametric dependence. The model identified in this way is valid inside a large range of temperatures and state-of-charge, so that the resulting model can be used for automotive applications such as on-board estimation of the state-of-charge and state-of-health. The model coefficients are identified using a multiple step genetic algorithm based optimization procedure designed for large scale optimization problems. The validity of the procedure is demonstrated experimentally for an A123 lithium ion iron-phosphate battery.



## 1. Introduction

In recent years, the use of hybrid powertrain technology has become a very effective method of improving fuel economy for automobiles. Vehicles with hybrid powertrains contain two or more separate power sources that are selected to complement each other as well as to provide added capabilities (such as regenerative braking) to improve the efficiency of the overall operation. Almost all commercial form of hybrid powertrain involves some combination of an internal combustion engine (ICE) and one or more electric machines (EM) (often referred to as hybrid electric vehicles, or HEV). While the ICE derives its power from fossil fuel, the EM obtains its energy from a battery pack. In order to minimize weight and size and still meet the energy and power demand while driving, typical battery cells have high power and high energy density. In older generations of HEVs (such as the Toyota Prius), nickel-metal hydride (NiMH) cells have been the battery choice due to their lower prices and good energy density. This choice is appropriate for HEVs that operate exclusively in a charge-sustaining mode, where the battery pack is maintained in a narrow range around a selected state-of-charge (SoC). Plug-in hybrid vehicles (PHEV) that require electric traction for extended periods, in a charge depleting mode, demand much more from the battery pack. In addition, their need for an all-electric range (AER) requires significantly more energy on-board. With the emergence of PHEVs, the vehicle electrification industry has opted to use the higher energy/power density lithium ion batteries.

Managing the battery pack for P/HEVs is a challenging problem. The objective of decreasing fossil fuel consumption while increasing drivability is in conflict with the objective of prolonging the life of the battery pack. If the full energy content of the battery pack is used, then clearly more gains are possible. However, the life of a rechargeable battery is significantly shortened when the battery is fully discharged or overcharged. In addition, overcharging (especially in the case of the lithium ion battery) can lead to catastrophic failure in the form of thermal runaway. Therefore, combining the objectives of improving fuel economy and drivability with battery life maximization dictates the requirement for careful SoC management of the battery. Furthermore, as batteries age, they become less able to store and supply energy. Consequently, the battery management system must be aware of the state-of-health (SoH) of the battery pack so that the vehicle control strategies can be adjusted accordingly. Having accurate models for use in estimating these critical characteristics, particularly for on-board vehicle application, therefore becomes an important requirement.

State-of-charge is commonly defined as the ratio between the amount of charge stored in the battery to the amount of charge that can be stored when the battery is fully charged. As such, SoC can be estimated by integrating the current going in and out of the battery pack. However, system noise and sensor calibration can render the electrical current measurement inaccurate, resulting in potentially large errors over time when that measurement is integrated. Another way to estimate the SoC is via the open circuit voltage

* Corresponding author. Tel.: +1 614 352 6605; fax: +1 614 688 4111.
*E-mail addresses:* yiran.hu@gmail.com (Y. Hu), yurkovich.1@osu.edu (S. Yurkovich), guezennec.1@osu.edu (Y. Guezennec), yurkovich.7@osu.edu (B.J. Yurkovich).

0378-7753/$ – see front matter © 2010 Elsevier B.V. All rights reserved.
doi:10.1016/j.jpowsour.2010.06.037

(OCV), taking advantage of the fact that a one-to-one mapping exists between the SoC and the OCV at a given temperature. However, the sensitivity of SoC to errors in OCV is very high due to the flatness of the OCV dependence on SoC for lithium ion batteries (see [1–3]). Because of various dynamics that characterize the battery behavior, a sufficiently accurate OCV can only be obtained after a long rest period (often several hours). This method for SoC estimation is therefore not realistic in real-time operation when the battery is constantly being used. Consequently, sole dependence on direct measurements typically does not produce accurate or useful estimates for SoC. SoH estimation is very similar to SoC estimation in terms of measurement difficulties. For example, a common way to quantify the SoH is via the capacity of the battery. However, as P/HEV batteries are never fully discharged, the capacity cannot be measured directly. In addition, any solution used to solve these estimation problems must be implementable on-board in real time, requiring only standard on-board measurements. This effectively rules out indirect frequency domain based ideas such as proposed in [4].

Of the many algorithms proposed in the literature to solve the SoC and SoH estimation problems (see [5] for a summary of basic algorithms used), model-based algorithms (such as extended Kalman filter [6,7] and sliding mode observers [8]) are attractive because they are efficient, robust, and do not require significant tuning, which is typical for numerically based methods such as artificial neural networks [9]. In order for model-based algorithms to be widely applicable, a control-oriented dynamic model is needed. The two types of models that are commonly used to describe the input-to-output behavior of a battery are electrochemical models [10] and equivalent circuit models [11]. Complexities of electrochemical models generally prohibit them from being used effectively in solving on-board estimation problems. Equivalent circuit models represent a simplification of electrochemical models by using electrical circuit elements to describe the battery behavior. For example, charge transfer across a boundary can be represented by a resistor in parallel with a capacitor, wherein ion diffusion can be represented by wave propagation on a transmission line. The appropriate construction of the equivalent circuit can be obtained via electrochemical impedance spectroscopy. Equivalent circuit models obtained this way are capable of exhibiting accuracy over a wide frequency range. However, very accurate equivalent circuit models tend to require distributed or nonlinear elements such as transmission line elements and Warburg impedances, which make on-board real-time application problematic. As seen in [12] however, battery responses at room temperature to typical current inputs seen in automotive applications can be approximated using an equivalent circuit that only contains resistors and capacitors. In such a model, circuit elements are scheduled on SoC and current direction. Models of this type are well suited for model-based algorithms. The primary shortcoming of the model presented in [12] is the fact that isothermal conditions were assumed. Because temperature can significantly affect battery behavior (such as increasing or decreasing the internal resistance), models that do not account for temperature change must themselves be scheduled or otherwise have limited use as part of a realistic on-board battery management system.

In this paper, the model in [12] is extended to include temperature dependence. The model is based on an equivalent circuit consisting of a voltage source and parallel resistor and capacitor circuits. Temperature dependence is addressed by allowing the model parameters to be dependent on temperature as well as SoC and current direction, resulting in a structure with a non-trivial number of unknown coefficients to be identified. These coefficients are identified in a multiple step genetic algorithm (GA) based optimization procedure, designed for large scale optimization problems. The identification procedure is discussed in detail for a modeling process with validation on an A123 lithium ion iron–phosphate battery.

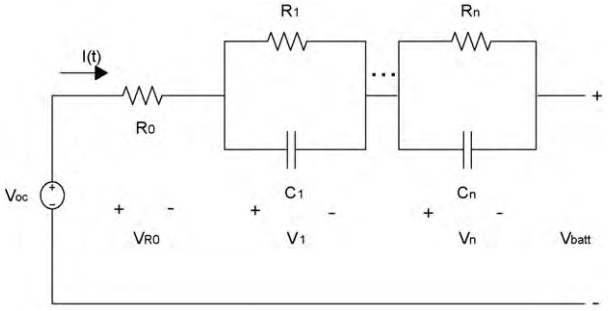


**Fig. 1.** Equivalent circuit used for battery model.

## 2. Battery model

Because the intended application for this model is for use in on-board estimation problems, the equivalent circuit structure employed herein will contain no distributed elements (such as transmission line) and nonlinear or pure frequency domain quantities such as the Warburg impedance. The resulting model structure may therefore be characterized using ordinary differential equations, where the specific structure selected is the Randle equivalent circuit shown in Fig. 1. The circuit is comprised of an ideal OCV, an internal resistance $R_0$, and $n$ parallel $RC$ circuits to approximate the battery dynamics. While not the most sophisticated model structure possible, this structure is selected because of its simplicity and universality. As reported in the earlier work [12], this structure provided a very good approximation for lithium ion battery dynamics at room temperature. Therefore, a natural next step is an extension to the case of multiple temperatures.

The dynamic equation that describes the voltage across the $i^{th}$ $RC$ circuit is given by

$$\frac{dV_i}{dt} = \frac{1}{R_i C_i} V_i + \frac{1}{C} I. \tag{1}$$

For convenience in identification, this equation can be viewed as a first order dynamic system in the form

$$\frac{dV_i}{dt} = -A_i V_i + A_i B_i I, \tag{2}$$

where $A_i = 1/(R_i C_i)$ and $B_i = R_i$ are the inverse of time constant and input coefficients, respectively. For now, $R_i$ and $C_i$ (consequently $A_i$ and $B_i$) are assumed to be dependent in some fashion on operating conditions. The precise nature of this dependence, and its justification, are discussed later.

The OCV in this equivalent circuit model is a function of the SoC. Technically, the OCV can have small variation with respect to the temperature. However, in experimental data collected, this difference is inconsistent and very small, so in this work the OCV is not parameterized as a function of the temperature. The SoC variation for a fixed temperature has a particular form. That is, the battery terminal voltage drops quickly as the SoC approaches 0% and rises as SoC reaches around 100% [13]. In a relatively large transitional portion of the SoC, the relation is nearly linear, and throughout the region the OCV is a strictly increasing function of the SoC. Given these characteristics, the OCV is modeled herein by a double exponential function as

$$V_{oc}(z) = V_0 + \alpha(1 - \exp(-\beta z)) + \gamma z + \zeta\left(1 - \exp\left(-\frac{\varepsilon}{1-z}\right)\right), \tag{3}$$

where $z$ is the SoC in decimal form (i.e. $z \in [0,1]$) and $\alpha$, $\beta$, .., $\varepsilon$ are tunable parameters.

The second component of the battery model involves the capacity and the SoC. To address this, first define the nominal capacity $C_n$ of a battery to be the amount of ampere-hours that can be drawn from the battery at 1 C-rate discharge at room temperature after a full charge (this is accomplished using protocols specified by the manufacturer, typically constant current to a given maximum voltage followed by constant voltage for a set period of time) before the battery reaches its minimum terminal voltage. Then the SoC of the battery, denoted by $z$, can be defined using standard Coulomb counting as

$$\dot{z} = -\frac{1}{3600C_n} I. \tag{4}$$

Other than as a component of the model, this formulation of SoC is also used to compute the true SoC for experimental datasets used in modeling and validation. Note that over a long period of time, Coulomb counting becomes inaccurate as a method of tracking the SoC. However, when datasets are kept short and processed carefully (off line), the accuracy of this technique is adequate.

As noted in the literature [3], if a battery is excited and then allowed to relax for long periods of time, due to electrical fields inside the battery caused by charges aligned during the excitation as well as diffusion effects, the rested terminal voltage at the same SoC varies depending on the type, duration, and strength of the previous excitation. To adequately capture this phenomenon, a hysteresis voltage element is appended to the equivalent circuit. As the hysteresis voltage is only changed when the battery is being charged or discharged (i.e. when the SoC varies), the dynamic equation for the hysteresis should be stationary when input current is zero.

In this work, a first order equation is selected to model the dynamics of the hysteresis voltage $V_h$ in the manner

$$\dot{V}_h = \Gamma(T)|I|(H(z, sign(\dot{z}), T) - V_h) \tag{5}$$

where $\Gamma$ can be thought of as a hysteresis transition factor (i.e. how fast the hysteresis occurs) and $H$ is the maximum amount of hysteresis voltage that can occur for a given SoC ($z$) and temperature ($T$). Depending on whether the battery is being charged or discharged, the sign of $V_h$ as a contribution to the battery terminal voltage will differ. Therefore, $H$ is also a function of the current direction, indicated by $sign(\dot{z})$. To make the model more flexible, $\Gamma$ is allowed to be a function of temperature. This allows the maximum hysteresis to be reached at different rates for different temperatures. Note here that the absolute value of the current is multiplied by the transition factor $\Gamma$ so that if no current is being pushed or drawn, the hysteresis voltage does not change, which is consistent with the requirement discussed earlier. Also based on this equation, the maximum hysteresis voltage is reached faster if the current magnitude is higher, again consistent with the physical nature of the battery.

Finally, the battery terminal voltage can be expressed as the sum of all the voltage components discussed previously:

$$V_{batt} = V_{oc} - R_0 I - \sum_{i=1}^{n} V_i - V_h. \tag{6}$$

Note that the signs of the $V_i$ are selected based on the standard current convention (negative current means charging and positive current means discharging). The signs of the hysteresis voltages are selected to be the same as those of the $V_i$. This tacitly implies that $H$ is positive when discharging and negative when charging.

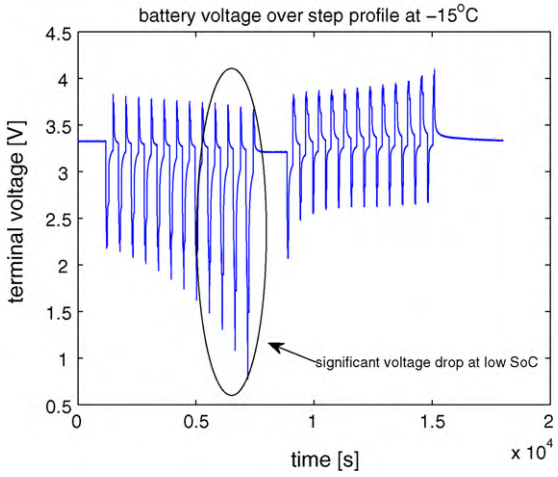


**Fig. 2.** Battery response to a series of asymmetric steps at −15 °C.

### 2.1. Parameter scheduling

Many parameters of the model formulated above depend on the operating conditions. The three primary operating conditions are determined by the current input, temperature, and SoC. Fig. 2 shows the voltage response of a test lithium ion battery being repeatedly excited with a set of asymmetric discharging and charging steps at −15 °C (data collection will be discussed in Section 4). In the first half of the dataset, the duration of the charging steps is only half to that of the discharging steps, thus causing the battery SoC to decrease gradually toward zero. The voltage response of the battery varies drastically between high SoC and low SoC, suggesting that coefficients describing the dynamics of the battery should be scheduled on SoC. Fig. 3 shows the same set of current steps for the battery at 5 °C; note that the responses at 5 °C differ significantly from those of −15 °C. Therefore, in the dynamic relationship of the model, parameters should also depend on the temperature. In the last half of the dataset shown in Fig. 2, a set of charging steps followed by a set of discharging steps is carried out, replicating the asymmetry used in the first half of the dataset. This allows the SoC of the battery to increase toward 100%. Clearly the response of the second half does not mirror that of the first half, indicating that the coefficients also depend on the current direction.

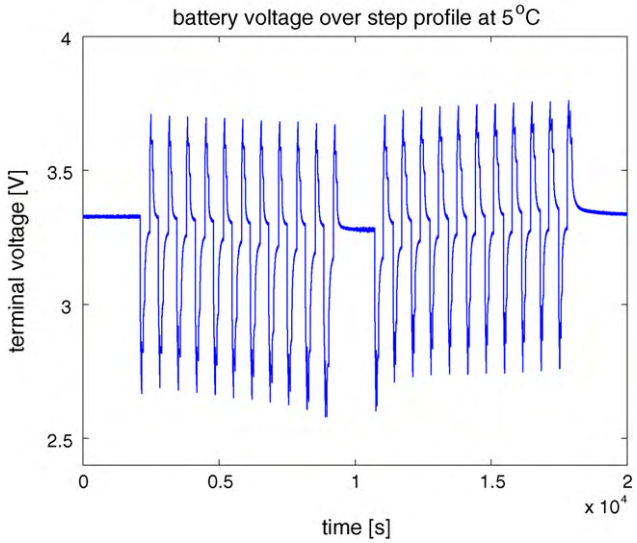


**Fig. 3.** Battery response to a series of asymmetric steps at 5 °C.

Because the exact dependence of the coefficients on the parameters is largely unknown and nonlinear, the functional form used for scheduling should be flexible enough to have no presumed shape, but at the same time should be convenient to define and evaluate. For the dependence on current direction, two sets of coefficients can be utilized, one for charging and one for discharging. Zero current behavior after charging will be considered charging, while zero current behavior after discharging is considered discharging. For the dependence on SoC and temperature, a typical solution is to use polynomial functions. While polynomial functions have the advantage of being smooth, their coefficients tend to be difficult to bound, which presents a challenge in parameter optimization for the coefficients. Therefore, instead of using polynomials, linear spline functions are used [14,15]. A linear spline function is a continuous piecewise linear function defined over a hypercube. To define a linear spline function, the function domain must be partitioned; by doing so in an arbitrarily fine manner, linear spline functions can be used to approximate any continuous function on that domain.

To construct a linear spline function, an arbitrary choice for the linear functions on each partition is not acceptable because of the continuity constraint; thus, a construction form is needed. This is obviously critical in a system identification algorithm as well, where a particular structure for coefficients is required. The standard representation for a linear spline function is via the so-called P-spline representation.

Let $s$ and $t$ be two independent variables (for example SoC and temperature). Without loss of generality, assume the domain of $s$ to be $[s_i, s_f]$ and the domain of $t$ to be $[t_i, t_f]$. Define the domain of $(s,t)$ to be the hypercube $[s_i, s_f] \times [t_i, t_f]$. Let a partition of $s$ be $[s_0 = s_i, s_1, \ldots, s_n = s_f]$ and let a partition of $t$ be $[t_0 = t_i, t_1, \ldots, t_m = t_f]$. Define functions $U_i$ for $i = 1, 2, \ldots, n$ as

$$U_i(s) = \begin{cases} s - s_i & s > s_i \\ 0 & \text{else} \end{cases} \tag{7}$$

Similarly define functions $V_j$ for $j = 1, 2, \ldots, m$ to be

$$V_j(t) = \begin{cases} t - t_i & t > t_i \\ 0 & \text{else} \end{cases} \tag{8}$$

If $f(s)$ is a linear spline function with the partition given for $s$, then $f(s)$ can be written uniquely as

$$f(s) = K_0 + \sum_{i=1}^{n-1} K_i U_i(s). \tag{9}$$

If $g(s,t)$ is a 2D linear spline function with the partitions given for $s$ and $t$, then $g(t,s)$ has a unique representation

$$g(t, s) = J_0 + \sum_{i=1}^{n-1} J_i U_i(s) + \sum_{j=1}^{m-1} L_j V_j(t). \tag{10}$$

The P-spline construction provides a very convenient way of evaluating a linear spline. Given $s$ and $t$, first evaluate the basis functions $U_i(s)$ and $V_j(t)$. Then (9) and (10) can be used to calculate the spline value for 1D and 2D splines, respectively. However, when searching for the best fitting linear spline to some data, bounds must be specified for the coefficients $K_i$ or $J_i$ and $L_j$. This can be difficult to do because these coefficients are essentially slopes. Another equivalent form exists where the spline function is specified via the values of the spline functions. For 1D splines, if the values of the spline functions are given on the knots, then the spline function is fully specified. For 2D splines, if the values of the function are specified on the knots around the left and lower boundaries (see Fig. 4 for an illustration), then the spline is fully specified. These facts can be proved by noting that (9) and (10) evaluated at the locations

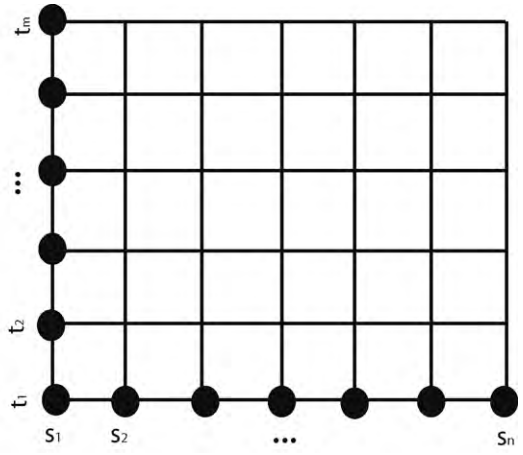


**Fig. 4.** Values needed to fully specify a 2D linear spline function.

described provide an invertible map between the values and the spline coefficients as long as the spline knots are distinct (which is assumed in our case). This *value form* of the linear spline function is convenient for identification because one can often find reasonable bounds for the coefficient values.

Using this formulation, the coefficient dependence on operating conditions can now be expressed. Table 1 depicts the parameter dependence of the model coefficients. Because the precise dependences of $A_i$, $B_i$, $H$ and $\tau$ on SoC and temperature are unclear from a physical perspective, all are considered to be generic functions of SoC and temperature. However, experimentation has shown that $\tau$ changes very little with respect to the SoC; therefore, in the interest of limiting the number of unknowns to be optimized, $\tau$ is selected to be a function of temperature only. Coefficients that depend on both SoC and temperature employ a 2D linear spline parameterization, whereas those that only depend on temperature use a 1D linear spline representation. Because the dynamic equations are linear (the algebraic output equation contains the only nonlinearity), the overall system with these parametrized coefficients is a quasi-linear parameter varying system [12].

## 3. Model identification

The model represented by (2) through (6) contains a large number of unknown coefficients that must be identified. Because the model is a continuous time differential equation in state variable form with nonlinear elements (though only in the output), approaches such as least squares [16] or subspace identification [17] used for linear parameter varying discrete systems are not easily applicable. Instead, the coefficients will be identified using an optimization procedure where the objective is to minimize the error between the measured battery terminal voltage and the model terminal voltage. The cost function to be minimized is the sum of squared errors at the sample points. As reported previous work [12], this choice of the error metric produces good results when compared with various other norms.

**Table 1**
Coefficient parametric dependence.

| Coefficient | SoC | Temperature |
|---|---|---|
| $A_i$ | × | × |
| $B_i$ | × | × |
| $H$ | × | × |
| $\tau$ | | × |

### 3.1. Input design

The first step in any model identification exercise is usually to collect physical data from the system being modeled. The data must be such that the model coefficients resulting in the best fit based on this data produce the best approximation to the battery dynamics. In this particular case, the dataset should obviously contain the entire range of SoC and temperature being modeled. While joint variation of SoC and temperature is certainly possible, temperature measurements tend to be inaccurate in a dynamical setting. Therefore a good approach is to grid the temperature space into several distinct temperatures. Then for each temperature, design a dataset that traverses the SoC range of interest. This obviously assumes that the battery behavior is continuous over temperature variations, so that for temperatures in between the gridded temperatures, interpolation produces accurate results. For datasets at each fixed temperature, the input signal should span all relevant time scales; as reported in [12], combinations of asymmetrical steps and pulses are a good choice. A dataset constructed in this way is representative of the type of data commonly seen in P/HEV operation, and is conducive for use with a variety of testing equipment (unlike white noise, chirp or some other signals commonly used for model identification). By including steps and pulses of various amplitude and duration, the dynamics described by the model can be excited sufficiently.

### 3.2. Optimization

The coefficient identification procedure uses a genetic algorithm based optimization routine, and is based on the process used for single temperature model identification. That is, the identification process is broken down into two segments: first identify a constant parameter model for that temperature; then use this constant parameter model as the starting point to find the SoC-dependent model. This two-step process is utilized to deal with the large number of unknowns that characterize the fully parameterized model. This basic procedure is modified for the multi-temperature case as follows:

1. Choose a desired model order. Then design and collect modeling datasets at different temperatures, including one at room temperature.
2. Apply single temperature identification for the room temperature dataset. This not only provides a model for the specific condition represented by that dataset, but also provides an open circuit voltage function to be used for other temperatures.
3. Using the OCV function identified for the room temperature dataset, identify the dynamic model equation coefficients for the other temperatures. Because the OCV is not dependent on temperature, the OCV curve is found once.
4. Interpolate the single temperature models using linear spline functions. In other words, if a coefficient is dependent on both SoC and temperature, then perform a secondary least squares fitting of a 2D linear spline function using the identified single temperature coefficients as the data. If a coefficient is not dependent on SoC but is different for each temperature, then a 1D linear spline is used.
5. Perform a global optimization over all the datasets using the interpolated coefficients as the starting point. While some single temperature coefficients are very smooth with respect to temperature, others are not. Thus, in a sense the interpolation process degrades optimality of the model coefficients. Therefore, it is important to re-optimize the coefficients jointly to regain global optimality.

The most important feature of this identification procedure is that prior to each optimization step, a good initialization is always available. For a global model with hundreds of unknown coefficients, lack of good initialization will often prevent the optimization from finding a useful solution.

### 3.3. Numerical considerations

An unforeseen numerical issue surfaced during the global optimization process in this work. When using the value form of the 2D linear spline functions (recall that this is basically the value of the function on the knots along the left and bottom boundary) to optimize for the coefficients, the values of the linear spline function on the top right corner can exceed the appropriate boundaries, especially for $R_0$ and $B_i$. Physically, this is because the internal resistance of the battery tends to grow in a rapid fashion as temperature and/or SoC decrease. The rate of this decrease is nearly exponential. As such, sometimes the values of these coefficients as identified can become either too large or even negative at some locations, despite being well bounded on the left and bottom boundaries. A simple and yet effective solution to resolve this issue is to prescale these coefficients via a monotonically increasing function. In this case, because the parametric variation shows an almost exponential trend, a log function is used. For example, rather than identifying $R_0$, it is more convenient to identify $\log(L \times R_0)$, where $L$ is a convenience factor that is used to make $\log(L \times R_0)$ positive. An additional advantage of using this prescaling is that the log version reduces the effect of outliers. Therefore it also acts as a filter of sorts so that the least squares fit during the interpolation step is more balanced. Note that this idea is not exclusive to linear spline functions. For example, this prescaling concept can be applied to polynomial functions, which are even more difficult to keep inside a boundary because of sensitivity to certain coefficients.

## 4. Model construction and validation

In this section, the results of a modeling exercise for a single cell lithium ion battery are presented. The battery used is an A123 lithium ion iron–phosphate cell (model 26650) with nominal capacity of 2.3 Ah and nominal voltage of 3.2 V. While not used on a wide scale in automotive applications (which focus more today on large capacity prismatic cells), this battery is easily available and has been widely evaluated for many different types of applications (hence does not involve issues of working around proprietary information). However, the procedure described here applies equally to other lithium ion cells. The temperature range of interest selected is from $-15\,^{\circ}$C to $45\,^{\circ}$C. The SoC region of interest is selected to be from 15% to 90% for temperatures at or higher than $0\,^{\circ}$C and 25% to 90% for temperatures below $0\,^{\circ}$C. This particular choice of SoC is due to the difficulties in operating the battery at lower temperature in the low SoC region. For example, at $-15\,^{\circ}$C and 20% SoC, even discharge at 1 C rate for a few seconds will cause the battery voltage to drop drastically below the factory specified minimum of 2 V. Therefore, designing a dataset for low SoC and low temperature is impractical unless very small currents are used. Furthermore, in practical automotive applications (even PHEV), the battery is not operated in the low temperature, low SoC region; therefore, this limitation does not detract from the utility of the model.

### 4.1. Experimental setup and data collection

The experiments were carried out in the battery characterization and aging laboratories at the Center for Automotive Research. This laboratory contains multiple stations capable of running tests of arbitrary lengths and can accommodate 24/7 unattended operation if needed. Each station testing a single cell or module is based

on a pair of programmable load and power supply, a data acquisition and control computer and Peltier junctions and associated controllers to provide a controlled thermal environment for the battery specimen under test for temperatures ranging between −25 °C and +60 °C. Each experimental station consists of an 800 W programmable electronic load and a 1.2 kW programmable power supply. The load and supply are controlled by a dual core computer running two instances of Matlab. The first instance is responsible for process control (monitoring and running the desired current profiles and built-in safety features). It is designed to allow for multi-day testing with error checking and text-messaging (SMS) services. The second instance is solely responsible for data acquisition. This experimental setup is a member of a large cluster of identical stations that allow for large scale battery testing and distributed data acquisition. The battery voltage is measured at the terminals of the battery at a sampling rate of 10 Hz. To ensure very tight tolerance on the battery temperature under any current profile, each test specimen is fixed in a specially machined aluminum plate with a large thermal mass, sandwiched between the Peltier junctions. The testing stations are calibrated on a regular basis to guarantee the best possible sensor measurements. The calibration data is used in the post processing of the testing data.

Data collection for multi-temperature modeling is in itself an art. Because the true SoC of the dataset can only be calculated via current integration, the initial condition of the SoC must be assessed carefully. Thus, prior to collecting each dataset, the battery is always charged to 100%. The charging process specified by the manufacturer is only valid for room temperature. If the same procedure is applied when the battery is at a different temperature (particularly the very low temperatures), the result of the charge can be significantly different from the same process at room temperature because the battery accepts charge differently at different temperatures. Therefore, to keep the datasets as uniform as possible, the process of charging to 100% is always carried out after the battery has been soaked at room temperature for 3 h. After the charging is completed, the battery is soaked at the desired testing temperature for three hours before any test is run. This is the only way of guaranteeing that the initial SoC is always known. Furthermore, the 3-h rest prior to the starting of the experiment ensures that the battery is at rest to begin the experiment. In this way, the initial conditions for $V_i$ and $V_h$ can be taken to be zero.

### 4.2. Current profile

Two types of current profiles are used to calibrate the model coefficients. The first is a series of asymmetrical step profiles (one typical period of the step is shown in Fig. 5). This profile is designed to allow the SoC of the battery to travel from the high limit to low limit (Fig. 6) with current steps as large as 6 C and as low as 2 C. This type of profile is used to emulate battery excitation during PHEV operations. The alternating charging and discharging steps, and alternating periods, provide sufficient excitation to correctly identify the coefficients. The asymmetrical profile is performed for each temperature. A second type of current profile used is the pulse profile, where symmetrical charge and discharge pulses (Fig. 7) are performed around several nominal SoC values, between 50% and 90% SoC (Fig. 8). The purpose of this profile is to emulate HEV charge-sustaining operations. The magnitude of the pulses range from 2 C to 16 C, which is characteristic of the rates seen in HEV operation. The pulse profile is only performed for temperatures above 15 °C because at lower temperatures, the higher internal resistance of the battery causes over-voltage. Note that in vehicle operation, battery packs are typically temperature controlled, so that it is unlikely that a battery will need to supply high currents at very low temperature.

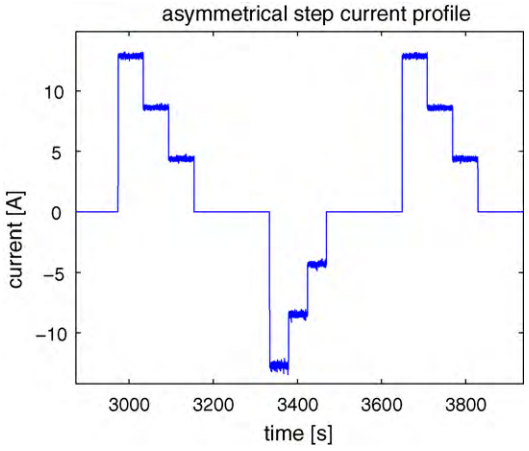


**Fig. 5.** Typical period of the asymmetrical step current profile.

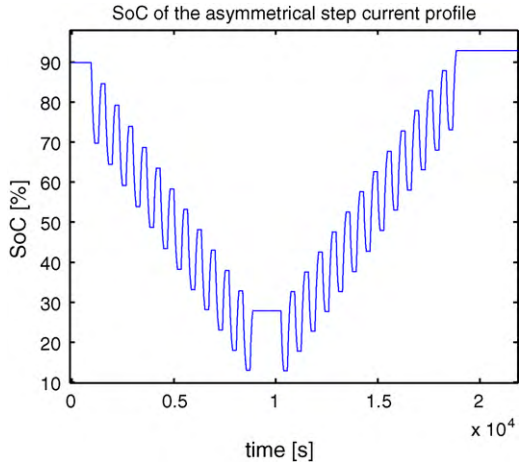


**Fig. 6.** SoC due to the asymmetrical step current profile.

### 4.3. Model identification

The order of the model is selected to be three so that a duration of three time constants can be represented. The SoC partition for the parameter space is selected to be [10, 15, 20, 25, 35, 45,

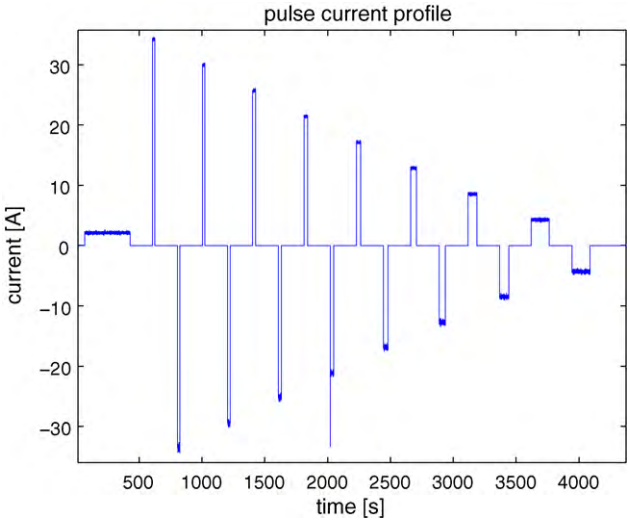


**Fig. 7.** Typical period of the pulse current profile.

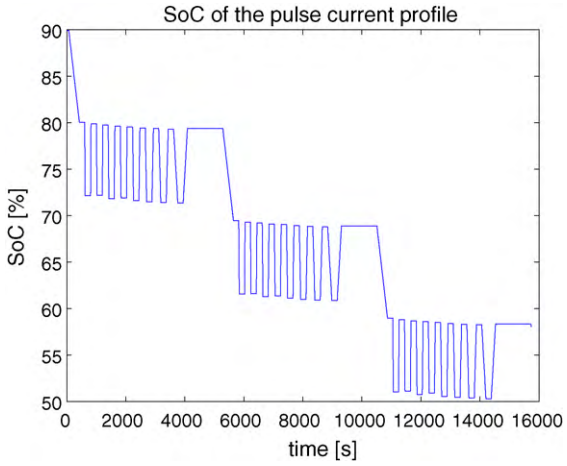


**Fig. 8.** SoC due to the pulse current profile.

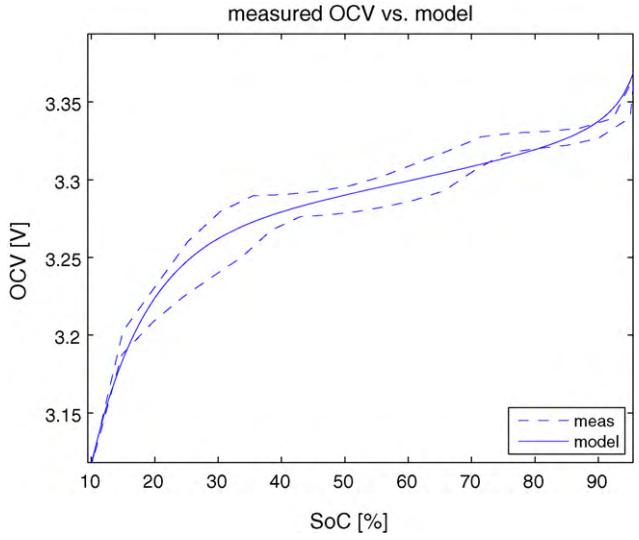


**Fig. 10.** Identified open circuit voltage compared with the measured.

60, 70, 75, 80, 85, 90] and the temperature partition is selected to be [−15, −10, −5, 0, 5, 15, 25, 35, 45] (temperatures at which data is collected). First, the room temperature model is identified, resulting in a model with very good agreement to both the step and pulse profiles; see Fig. 9 where the model result (solid line) practically lies atop the measured (dashed), with 15 mV of RMS error. Because the OCV curve identified at room temperature (25 °C) is to be used for all subsequent identifications, the identified curve is compared to a measured curve. The OCV measurement is done by repeated discharges of 5% of the SoC with an hour of rest afterward to relax the dynamics, after which a mirror charging process is performed. Because of hysteresis and long battery dynamics, after an hour of rest the OCV is not the true OCV. Therefore the voltage measured during the discharging is taken to be a lower bound and the voltage measured during the charging is taken to be an upper bound. As Fig. 10 illustrates, the identified OCV resides between the two measured curves, providing a level of confidence that the room temperature model identification was successful.

The next step is to identify various single temperature models using the same process; except for the two lowest temperatures, the models fit the data very well. For the very low temperatures, the battery behavior is highly nonlinear, especially during discharge, as even small current over a short period produces a very large voltage drop, which the model has difficulty capturing. Nevertheless, prior to the voltage drop, the model still captures the battery behavior (more details later).

Next the identified single temperature model coefficients are fitted to 2D linear spline functions, after which the fitted coefficients are jointly optimized over all the temperatures. Figs. 11 and 12 show the internal resistances in charge and discharge respectively as functions of the SoC and temperature. Three things are immediately obvious from these two figures. First, the internal resistance shows a smooth increase as temperature decreases; which is consistent with physical explanations from an electrochemical analysis. Secondly, as the SoC increases toward 100% or decreases toward 0%, the internal resistance also increases, an effect that is especially clear at lower temperatures. This, too, is consistent with the observed data where the battery voltage either increases rapidly near 100% or decreases rapidly near 0%. Furthermore, the charge and discharge internal resistances show different behavior as they approach the extreme SoCs, as expected.

Table 2 summarizes the root mean square (RMS) errors of the model identified over the various datasets. RMS error is used because it has the units of volts, which is easy to visualize. From these results, two trends are obvious. As temperature decreases, the size of the error increases. This is primarily because the battery behavior becomes highly nonlinear as temperature decreases.

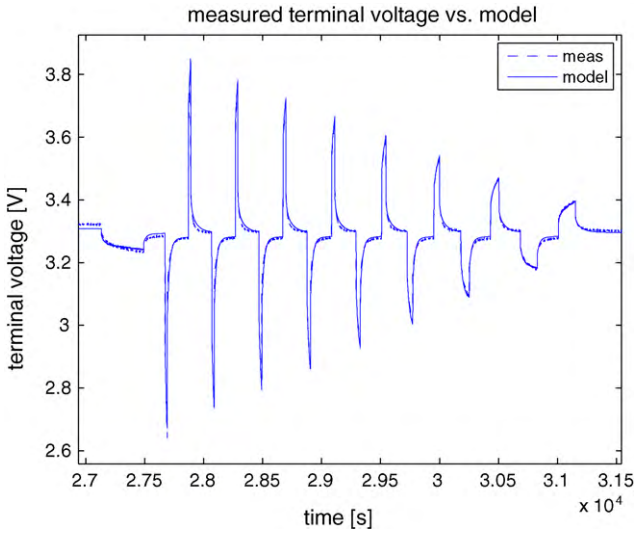


**Fig. 9.** Fit of the model to the pulse profile data at 25 °C (RMS error = 15 mV).

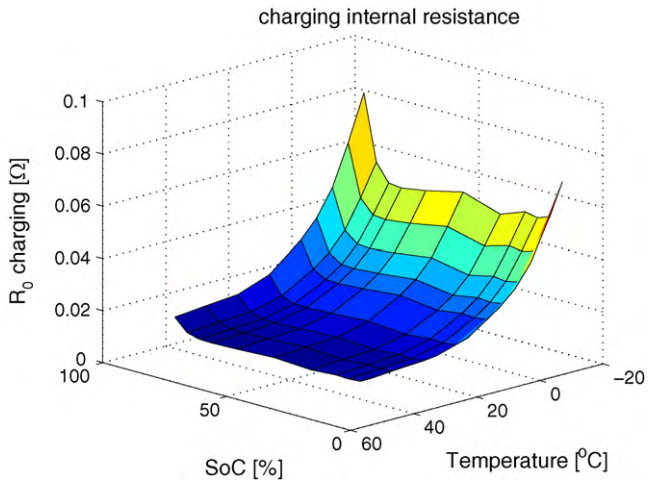


**Fig. 11.** Identified charging internal resistance as a function of SoC and temperature.

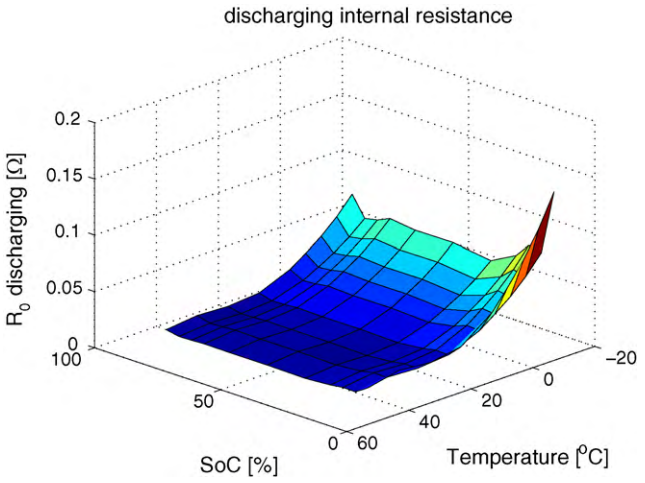


**Fig. 12.** Identified discharging internal resistance as a function of SoC and temperature.

**Table 2**
RMS error of the model over the modeling datasets.

| Temperature (°C) | Profile | RMS error (V) |
|---|---|---|
| −15 | Step | 0.081 |
| −10 | Step | 0.049 |
| −5 | Step | 0.036 |
| 0 | Step | 0.028 |
| 5 | Step | 0.018 |
| 15 | Step | 0.018 |
| 15 | Pulse | 0.014 |
| 25 | Step | 0.015 |
| 25 | Pulse | 0.013 |
| 35 | Step | 0.016 |
| 35 | Pulse | 0.011 |
| 45 | Step | 0.013 |
| 45 | Pulse | 0.010 |

Notice that from −5 °C to 45 °C, the size of the error is still very small for equivalent circuit models. As for the single temperature models, at −10 °C and especially at −15 °C, the model has difficulty capturing the voltage drop during the net discharging phase, as seen in Fig. 13 (once again, the model response is represented by the solid line, whereas the dashed line shows the measured data). However, as Fig. 13 also shows, the model fits the data well in other areas of

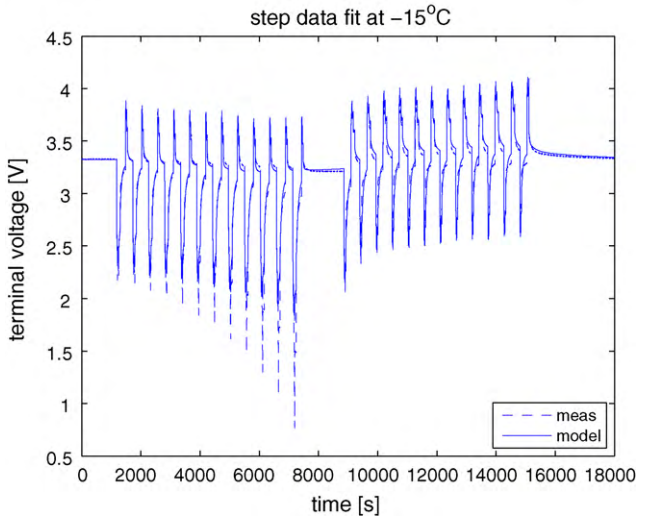


**Fig. 13.** Model fit for the step profile data at −15 °C.

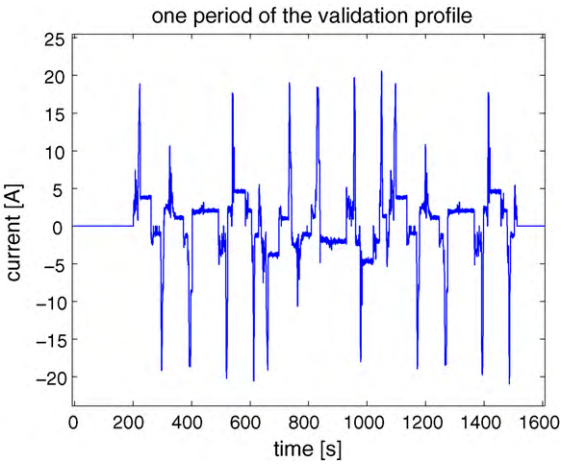


**Fig. 14.** Current profile for one measured driving sequence in the validation profile.

the profile. In the next section, validation exercises are illustrated for a different profile, but these results suggest that the model has captured dynamics sufficiently to be useful in estimation problems.

### 4.4. Model validation

To ensure that the battery model works well in realistic settings, a validation profile was created. In this profile, the temperature and SoC of the battery are simultaneously varied (note that the temperature control is done using an environmental chamber instead of Peltier junction because of its programmability). Initially, the SoC of the battery is set to 90%. Then the battery is soaked at −5 °C for more than 3 h. Next, a short driving cycle extracted from a measured HEV dataset is suitably rescaled as shown in Fig. 14. The current sequence was selected so that its net effect results in a 5% decrease in SoC. By repeating this cycle 12 times, the SoC of the battery is decreased from 90% to approximately 30% as shown in Fig. 15. Meanwhile, the temperature of the environmental chamber is slowly ramped up to 40 °C and then back down to 25 °C (Fig. 16). This profile simulates a common case of PHEV driving where a vehicle which has been parked overnight in subzero temperatures is used for commuting. The temperature rise corresponds to the temperature control on the battery pack in the vehicle warming up the battery after the vehicle is started. Because the temperature is varied continuously, this realistic profile can test the validity

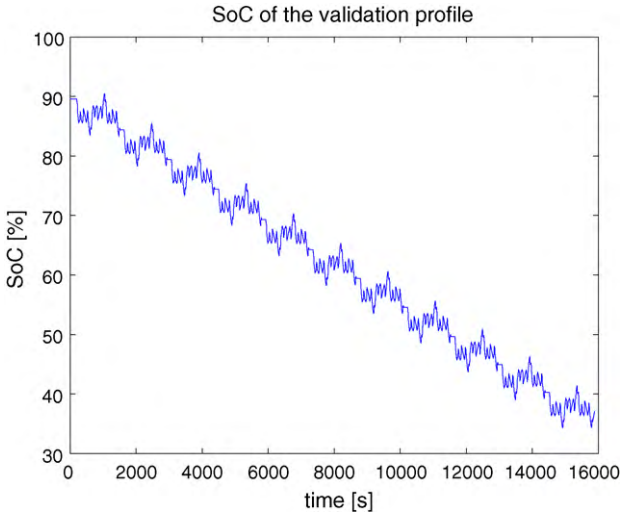


**Fig. 15.** SoC variation for the validation profile.

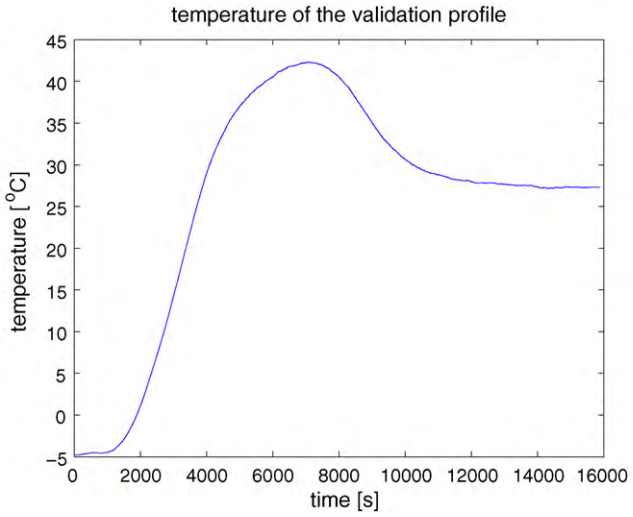


**Fig. 16.** Temperature variation of the validation profile.

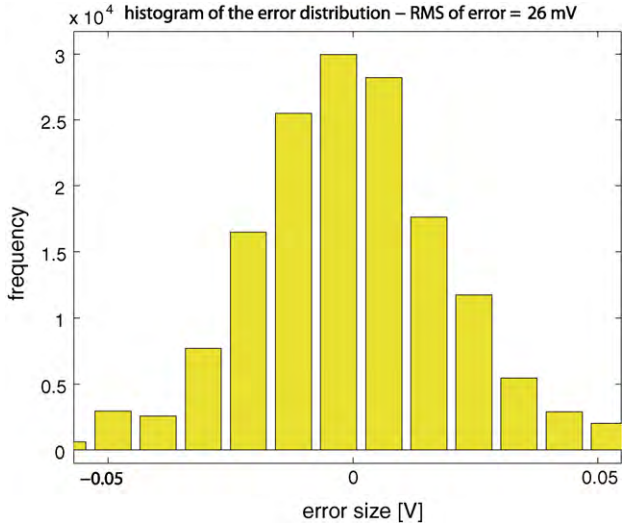


**Fig. 17.** Histogram of the error distribution over the validation dataset.

of the model at temperatures not specifically modeled. In other words, this procedure validates the interpolation process for the coefficients.

Over this entire profile, the RMS error in the model is less than 26 mV, which is very good for the temperatures considered; Fig. 17 shows the distribution of the errors in the form of a histogram. The distribution is Gaussian-like, suggesting that the model captured the desired responses. With errors of this size, model-based SoC and SoH estimators using this model can be designed with very good results.

## 5. Conclusion

In this work, a complete set of procedures is provided for identification of equivalent circuit battery models that can be used in automotive applications. The results of a modeling exercise conducted on an 26650 A123 lithium ion iron–phosphate battery show good response over a large range of SoC and temperature (on both the modeling dataset and a separate validation dataset). Because the model is a control-oriented model, various model-based algorithms used for SoC and SoH estimation problems can be readily adapted to use with this model. Furthermore, the model itself is useful in P/HEV simulators.

This approach to battery modeling offers several contributions. First, all parameters of the battery are identified from one rich dataset that contains the necessary parameter and temporal variations. Therefore the identification procedure is overall efficient and requires little user interaction. Secondly, the use of linear spline functions for model coefficient parametrization allows an assumption of arbitraty shapes for the coefficient functions, while being very easy to optimize. Finally, several useful and practical tips are presented to make data-taking systematic and accurate and to reduce undesired numerical issues that can occur during the identification process.

## References

[1] L. Serrao, Z. Chehab, Y. Guezennec, G. Rizzoni, Proceedings of the 2005 IEEE Vehicle Power and Propulsion Conference, 2005.
[2] S. Pang, J. Farrell, J. Du, M. Barth, Proceedings of the American Control Conference, 2001, pp. 1644–1649.
[3] M. Verbrugge, E. Tate, Journal of Power Sources 126 (2004) 236–249.
[4] A. Salkind, C. Fennie, P. Singh, T. Atwater, D. Reisner, Journal of Power Sources 80 (1999) 293–300.
[5] S. Piller, M. Perrin, A. Jossen, Journal of Power Sources 96 (2001) 113–120.
[6] G. Plett, Journal of Power Sources 134 (2004) 262–276.
[7] G. Plett, Journal of Power Sources 134 (2004) 277–292.
[8] I. Kim, Journal of Power Sources 163 (2006) 584–590.
[9] C. Cai, D. Du, Z. Liu, J. Ge, Proceedings of 7th World Congress on Intelligent Control and Automation, 2008.
[10] A. Ledovskikh, E. Verbitskiy, A. Ayeb, P. Notten, Journal of Alloys and Compounds 356–357 (2003) 742–745.
[11] E. Barsoukov, J.R. MacDonald, Impedance Spectroscopy: Theory, Experiment, and Applications, second edition, Wiley-Interscience, 2005.
[12] Y. Hu, S. Yurkovich, Y. Guezennec, B.J. Yurkovich, Control Engineering Practice 17 (2009) 1190–1201.
[13] D. Linden, T.B. Reddy, Handbook of Batteries, third edition, McGraw Hill, 2001.
[14] K. Dudek, Application of Linear Splines to Internal Combustion Engine Control, US Patent No. 7,212,915 B2.
[15] P. Dierckx, Curve and Surface Fitting with Splines, second edition, Oxford Science, 1993.
[16] B. Bamieh, L. Giarre, Proceedings of the 38th Conference on Decision and Control 42 (1) (2003) 76–97.
[17] V. Verdult, M. Verhaegen, Automatica 38 (2002) 805–814.